

## TWO METHODS FOR REMOTE ESTIMATION OF COMPLETE URBAN SURFACE TEMPERATURE

Lu Jiang<sup>a</sup>, Wenfeng Zhan<sup>a,b,\*</sup>, Zhaoxu Zou<sup>a</sup>

<sup>a</sup> Jiangsu Provincial Key Laboratory of Geographic Information Science and Technology, International Institute for Earth System Science, Nanjing University, Nanjing, Jiangsu 210046, China – jianglu\_v7@foxmail.com; zouzhaoxuy@126.com

<sup>b</sup> Jiangsu Center for Collaborative Innovation in Geographical Information Resource Development and Application, Nanjing, 210023, China – zhanwenfeng@foxmail.com

Commission IV, WG IV/3

**KEY WORDS:** Urban surface; Thermal anisotropy; surface temperature; complete urban surface temperature; Semi-hemispherical temperature; kernel-driven model.

### ABSTRACT:

Complete urban surface temperature ( $T_c$ ) is a key parameter for evaluating the energy exchange between the urban surface and atmosphere. At the present stage, the estimation of  $T_c$  still needs detailed 3D structure information of the urban surface, however, it is often difficult to obtain the geometric structure and composition of the corresponding temperature of urban surface, so that there is still lack of concise and efficient method for estimating the  $T_c$  by remote sensing. Based on the four typical urban surface scale models, combined with the Envi-met model, thermal radiant directionality forward modeling and kernel model, we analyzed a complete day and night cycle hourly component temperature and radiation temperature in each direction of two seasons of summer and winter, and calculated hemispherical integral temperature and  $T_c$ . The conclusion is obtained by examining the relationship of directional radiation temperature, hemispherical integral temperature and  $T_c$ : (1) There is an optimal angle of radiation temperature approaching the  $T_c$  in a single observation direction when viewing zenith angle is  $45 \sim 60^\circ$ , the viewing azimuth near the vertical surface of the sun main plane, the average absolute difference is about 1.1 K in the daytime. (2) There are several (3~5 times) directional temperatures of different view angle, under the situation of using the thermal radiation directionality kernel model can more accurately calculate the hemispherical integral temperature close to  $T_c$ , the mean absolute error is about 1.0 K in the daytime. This study proposed simple and effective strategies for estimating  $T_c$  by remote sensing, which are expected to improve the quantitative level of remote sensing of urban thermal environment.

### 1 INTRODUCTION

Urban surface temperature (UST) is a variable crucial to the estimation of surface radiation and energy budgets, and it therefore plays an important role in the investigation of urban climate and environment (Voogt & Oke, 2003). Thermal infrared remote sensing (TIR) provides an indispensable way to obtain USTs at a large scale (Li et al., 2013). Nevertheless, this technique usually detects the surface thermal radiation (or temperature) in a certain or very few observation angles, i.e.,  $T(\theta, \varphi)$ , where  $\theta$  and  $\varphi$  are the viewing zenith and azimuth angles, respectively, while urban surfaces demonstrates significant thermal anisotropy during both the daytime and nighttime (Lagouarde et al., 2010; Lagouarde et al., 2012). It is thus rather difficult for the TIR technique to obtain a UST adequately descriptive to represent the true surface thermal status.

The estimation of the representative USTs requires the deep understanding of urban thermal anisotropy (UTA). Both field and airborne experiments as well as computer modelling have been used to understand the regime of UTA (Soux et al., 2004; Yu et al., 2006; Voogt, 2008; Lagouarde et al., 2010, 2012; Zhan et al., 2012; Ma et al., 2013; Allen et al., 2017). Their results show that, when compared with the natural surfaces dominated

primarily by vegetation, urban surfaces exhibit a more noteworthy hot-spot effect: The UTA intensity at noon can be as high as 10.0 K or more in a clear sky, but it decreases rapidly after sunset (Voogt, 2008; Lagouarde et al., 2010; Zhan et al., 2012). In view of the higher structural complexity of urban surfaces, kernel-driven models that are able to reconstruct radiation temperatures at all directions within the upper hemisphere using only several directional radiation temperatures (DRTs) have also been developed recently (Vinnikov et al., 2012; Sun et al., 2015; Duffour et al., 2016). These kernel-driven models are capable of modifying the DRTs into nadir temperatures and further have the potential to acquire a UST sufficiently representative of the urban thermal status.

Nevertheless, unlike the pure vegetation, nadir temperatures of urban pixels likely distort the radiation and energy exchange between the urban surface and the atmosphere. For this reason, Voogt & Oke (1997) proposed the concept of the complete urban surface temperature (termed  $T_c$ ), which was defined as a weighted summation of component surface temperatures multiplied by its associated component fractions from a three-dimensional perspective. When compared with  $T(\theta, \varphi)$ ,  $T_c$  served better on the estimation of surface fluxes (Voogt & Grimmond, 2000). In consideration of its better performance,  $T_c$  has been

---

\* Corresponding author

calculated directly according to its standard definition by combining detailed field measurements on component surface temperatures and fractions (Voogt & Oke, 1997; Voogt, 2000). Their results confirmed that there was a large difference between  $T_c$  and the nadir temperature, and preliminary analysis illustrated that the DRTs with more shadowed component areas contained in the observational field of view (FOV) would be closer to  $T_c$ . Further research indicated that the hemispherical radiation temperatures (HRTs) measured by pyrgeometers are better for approaching  $T_c$  (Roberts et al., 2009; Adderley et al., 2015).

Although preliminary progress has been made on the estimation of  $T_c$ , currently the remote estimation of  $T_c$  from airborne or spaceborne observations without the assistance of ground-based measurements remains challenging, mostly because of the difficulty to accurately quantify the component temperatures and fractions for complex urban surfaces from a remote sensing perspective. For the remote estimation of  $T_c$ , issues need to be solved in the following two aspects: (1) is there an optimal remote sensing observation angle (view) that is close to  $T_c$  in a single observation angle? (2) In the case of radiation temperatures with several viewing angles, can the hemisphere integral temperature reconstructed by the thermal infrared kernel model, be used to approximate the  $T_c$ ?

To answer these two questions, based on the simplified scale model of typical urban surface with different height width ratio (Building-Height-to-Spacing-Width ratios, H/W), this paper calculates  $T(\theta, \varphi)$  in each viewing angle of urban surface by computer simulation, seeks for the optimal viewing angles approaching  $T_c$ , and further explores the possibility of directly approaching  $T_c$  by kernel model with several directional radiation temperatures. In order to obtain the accurate method for the estimation of  $T_c$  by remote sensing under various observation scenarios, this paper supports the improvement of

the quantization level of urban environment remote sensing.

## 2 DATA AND METHODS

### 2.1 Scale model for typical urban surfaces

The geometric structure of urban surface is complex, and the building density, building height and street width have a direct impact on urban surface temperature.

In order to include all kinds of typical urban surface types, this paper puts forward the local climate zoning (LCZ) according to Stewart and Oke (2012), 3ds-Max software is used to design four kinds of physical scale models of three dimensional structure of typical urban surface called typical urban surface(TUS)(Fig.1) which with different building density (dense or sparse distribution), building height (high, low or mixed layer): TUS01 is a densely distributed group of tall buildings (such as a city center, a business district, etc.); TUS02 is sparsely distributed low rise buildings (such as urban light industrial or residential areas); TUS03 is a sparse distribution of high and low buildings (e.g. City, commercial, residential, mixed, etc.); TUS04 is a large sparse building with sparse distribution (such as large workshop type industrial district). The surface geometry and other related parameters of the four physical scale models are shown in Table 1.

### 2.2 Simulation of component temperature

Urban microclimate software Envi-met, one of the mainstream of urban environment and microclimate simulation software, its simulation of the surface temperature effect is good (Chow et al., 2011; Huang et al., 2015), it will mainly use Envi - met simulate urban surface temperature (components temperature). Compared

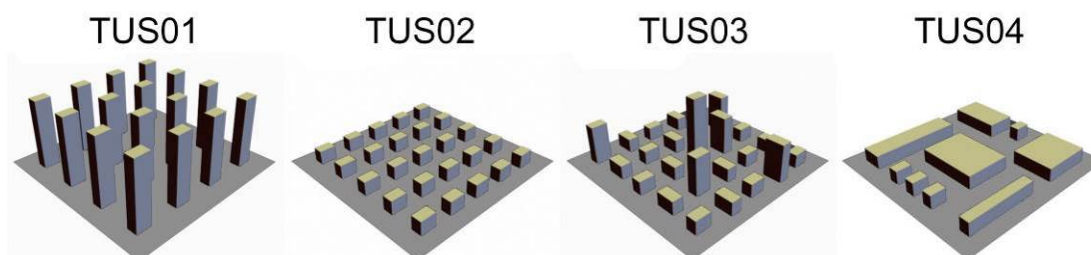


Fig.1. Scale models of four typical urban surfaces (TUS).

**Table.1.** The geometric structure parameter information of four types of urban underlying surface model includes the building type, building height and street width ratio (H/W), and the surface area of the ground surface, which accounts for the weight of the whole surface.

Scale model (TUS)	Building heights	Aspect ratio (H/W)	Wall (%)	Roof (%)	Street (%)
TUS01	20-25 stories	2.6	64	3	33
TUS02	4-6 stories	0.8	36	8	56
TUS03	4-25 stories	0.7-5.0	51	8	41
TUS04	4-6 stories	0.3-1.0	35	24	41

to the spring and autumn season, urban underlying surface thermal radiation directivity characteristics more typical representative in summer and winter (Lagouarde et al. 2010), and the main consideration two seasons (summer and winter) in this paper. On the basis of the foregoing city of building physical scale model, we simulate the surface temperature of Nanjing, China (118.54 °E, 31.56 °N) in four types of physical scale

model in a whole day and night cycle in summer and winter.

The physical scale model of TUS03 as an example, there is a complete description of a day cycle in summer, the input parameters using Envi-met simulation required: (1) the simulation area of 240 m×240 m, according to the characteristics of Envi-met numerical simulation model, is set to 60×60×30

mesh. The grid resolution were  $dx=4$  m,  $dy=4$  m and  $dz=6$  m ( $dx$  and  $dy$ , horizontal resolution of  $X$ ,  $Y$ ;  $dz$ , vertical resolution of  $Z$ ). (2) The simulation start time is set in July 29, 2015 (winter time is January 15, 2016) 06:00, and the simulation lasts 24 hours. (3) Meteorological forcing data using the site measured value, the initial air temperature is 26 °C (06:00 measured average), with the prevailing southwest wind (wind direction azimuth angle is 240°), 10 m height wind speed was 1.0 m/s (measured average value), the relative humidity is 90% (measured).

Under the influence of solar radiation, the urban surface temperature in daytime and shadow is different greatly, and the trend of the surface temperature of different building faces is different. In order to better carry out radiation forward simulation heat according to the statistical characteristics of the surface temperature of the building facade in different city, the city is divided into surface light / shadow under the ground, the east wall, west wall, south wall, north wall, roof (a total of 12 kinds of component types (Zhan et al. 2012). The surface temperatures of the 12 types of components are calculated directly by the mesh surface temperature of the Envi-met simulations.

### 2.3 Forward simulation of directional radiation temperature

On the basis of the aforementioned urban surface physical scale models and component temperature as input, in this paper, the directional radiation temperature  $T(\theta, \varphi)$  of the urban surface in the upper hemisphere (the observation position of sensor, zenith angle is 0~90°(interval set to 10°), and azimuth is 0~360°(interval is set 30°)) is calculated directly by using the CoMSTIR (Computer Model to Simulate the Thermal Infrared Radiation of 3-D urban targets) model of urban surface thermal radiation. The model of CoMSTIR has a more rigorous physical basis, and its simulation result precision (RMSE) reaches 0.7 K (Ma et al., 2013). The geographical location information (longitude and latitude), observation time, sensor space position parameters are required, when  $T(\theta, \varphi)$  is simulated by CoMSTIR.

### 2.4 Simulation of directional radiation temperature by kernel model

By means of surface thermal radiation direction of nuclear driven simulation model proposed by Vinnikov et al. (2012) (hereinafter referred to as Vinnikov model), on the basis of only a few known  $T(\theta, \varphi)$ , the  $T'(\theta, \varphi)$  in all directions of the upper hemisphere is reconstructed. The semi-empirical statistical model—Vinnikov model ponders the surface temperature changing with angle under the "Sensor - Target - Sun "three different relative position relation, has higher accuracy (RMSE value less than 1 K), is suitable for the simulation of city surface thermal anisotropy (Sun et al., 2015; Duffour et al., 2016).The model can be expressed by the following simple equation:

$$T(\theta, \theta_i, \Delta\varphi) = T_0 \cdot [1 + A \cdot \Phi(\theta) + D \cdot \Psi(\theta, \theta_i, \Delta\varphi)] \quad (1)$$

where,  $\theta$ ,  $\theta_i$  with  $\Delta\varphi$  are sensor viewing zenith angle, solar zenith angle and sun-sensor relative azimuth angle;  $T_0$  is nadir radiance temperature; A and D are coefficients of kernel driven model;  $\Phi(\cdot)$  and  $\Psi(\cdot)$  are the "the emissivity kernel" and "the solar kernel".

### 2.5 Calculation of integral temperature and complete surface temperature

Hemispherical Angle Integral temperature ( $T_H$ ) for the specific direction of solid angle range  $\Omega$  radiation temperature  $T(\theta, \varphi)$  integral, its computation formula is as follows:

$$T_H(\Omega) = \iint_{\Omega} T(\theta, \varphi) d\Omega \quad (2)$$

Complete surface temperature ( $T_c$ ) is not obtained by direct observation, can be expressed as component temperature ( $T_i$ ) and component area completely weight ( $f_i$ ) of the surface of a weighted sum, of the product of specific calculate formula is as follows (Voogt & Oke, 1997):

$$T_c = \sum_i^n f_i T_i \quad (3)$$

The number of components of  $n$  is in the form (the 12 components are set in section 2.2).

### 2.6 Remote sensing estimation/approximation strategy of $T_c$

#### 2.6.1 Single direction observation

In order to obtain the  $T(\theta, \varphi)$  of optimal angle which close to  $T_c$  under the single direction observation by remote sensing, we will use CoMSTIR to simulate four typical urban surfaces (TUS01~TUS04), 24 day time intraday (hourly), 2 typical seasons (summer and winter), and get a total of 192 polarization diagrams of  $T(\theta, \varphi)$  (i.e. Zenith angle range of 0~90°; the azimuth angle is in the range of 0~360°). The  $T(\theta, \varphi)$  which is closest to  $T_c$  in the mean sense, is comprehensively investigated.

#### 2.6.2 Multi-directional observations

In order to obtain a remote sensing estimation / approach  $T_c$  method in a multi direction observation scenario, the  $T_H(\Omega)$ , which is closest to  $T_c$  in the mean sense, is evaluated in a comprehensive manner. The  $T_H(\Omega)$  including  $T_H(0\sim0^\circ, 0\sim360^\circ)$  (i.e. nadir radiation temperature, the follow-up will be directly marked as  $T_0$ ),  $T_H(0\sim30^\circ, 0\sim360^\circ)$  (marked as  $T_{h30}$ ),  $T_H(0\sim60^\circ, 0\sim360^\circ)$  (marked as  $T_{h60}$ ),  $T_H(0\sim90^\circ, 0\sim360^\circ)$  (i.e. hemisphere integral temperature, marked as  $T_{h90}$ ), and  $T_{oa}$  (optimal view angle direction radiation temperature). In addition, 4 observation angles with more uniform distribution are selected, including (20°, 30°), (40°, 120°), (50°, 330°) and (60°, 240°). Based on the  $T(\theta, \varphi)$  at these angles, the radiation temperature  $T'(\theta, \varphi)$  in each direction is reconstructed by the Vinnikov model (in section 2.4), and the capability of approximating the  $T_c$  with the optimal hemispherical angle integral temperature calculated on the basis of  $T'(\theta, \varphi)$  is investigated.

## 3 RESULTS

### 3.1 Comparison of $T(\theta, \varphi)$ and $T_c$

The polar-DRT of directional radiation temperature  $T(\theta, \varphi)$  of daytime typical time of summer and winter over the scale model and contour of  $T_c$  as shown in Fig.2. Due to limited space, here offers only a polar-DRT of scale model TUS03 on the typical time (09:00, 13:00 and 17:00) in summer and winter, the rest polar-DRTs of scale models as shown in APPENDIX A. The simulation results show that, the thermal anisotropy of urban surface in the daytime of winter and summer and "hot spot

"effect (the azimuth of "hot spot" is close to sun's) is obvious. At 13:00 of summer, corresponding to the zenith angle of "hot spot" is about 30°(Fig.2.b), and the zenith angle of "hot spot" of the rest of 09:00 and 17:00 of summer and three-time of winter is close to 90°respectively, this may because of at summer noon (13:00) of the solar zenith angle is much smaller than others shown in the figure.

As shown in fig.2, the value of  $T_c$  is between the maximum and minimum values of  $T(\theta, \varphi)$ , and is relatively closer to the minimum value of  $T(\theta, \varphi)$ . The contour line of  $T_c$  occasionally approximates the nadir radiation temperature  $T_0$ , for example,

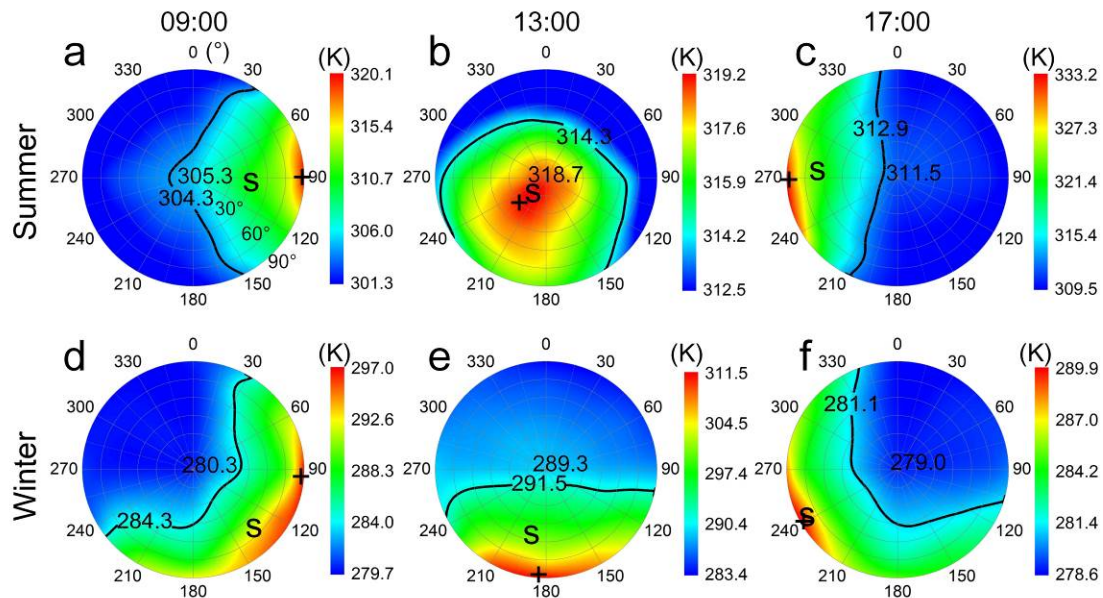


**Fig.2** The polar-DRT of daytime typical time of summer and winter over the scale model (TUS03) and contour of  $T_c$  (unit K). The black cross indicates the position of "hot spot", the "S" indicates the position of sun. And, (a), (b) and (c) are in summer, (d), (e) and (f) are in winter, the zenith angle and azimuth range are 0~90° and 0~360° respectively.

### 3.2 Optimal angle of $T_c$ under a single direction

As far as the single temperature polarization diagram is concerned, the zenith angle and azimuth angle of the contour of  $T_c$  can be considered as the best observation angle of approaching  $T_c$ . In order to find the optimal angle (sight) for all scale models and moments can approximate  $T_c$ , we integrate the contours of  $T_c$  in the polarization graph of  $T(\theta, \varphi)$  of all scale models at a particular moment, and obtain the contour (the best viewing angle) set of approaching  $T_c$  (Fig.3). Considering the difference of the sun position between winter and summer, we rotate the solar main plane (temperature polarization diagram) corresponding to the winter to the position of the solar main plane in summer (S - S').

As seen from Fig.3, the contours of  $T_c$  converge closely in or around the elliptical dotted line in the figure, that is, the position indicated by the dotted circles are the optimal angle field approaching the  $T_c$ . For the different times in the daytime (Fig.3), the marked dotted circles are roughly located near the vertical plane of the solar main plane, that is, the azimuth angle of optimum observation is approximately equal to the solar azimuth  $\pm 90^\circ$ , and the zenith angle of optimum observation is about 45~60°. TUS03 still as example, at 11:00, 13:00 and 15:00 in the summer, compare the temperature value of  $T(60, 180)$ ,  $T(60, 300)$  and  $T(60, 330)$  in (or near) dotted circle to  $T_c$  which the corresponding time, the difference  $|\Delta T|$  is only 0.49, 0.37 and 0.27 K, respectively (for the simulated temperature value by

the difference is only 1.0 K at 09:00 in summer. However, there may also be significant differences between  $T_0$  and  $T_c$ , and  $T_0$  can not simply replace  $T_c$ . The physical scale model of LCZ03 as an example, at 13:00 of summer and 09:00 of winter, the difference of  $T_c$  and  $T_0$  can be up to 4.4 and 4 K. The simulation results for all physical scale models and all day time further show that the range of  $\Delta T$  is up to 6.0 K (LCZ01; at 17:00 of summer), the average absolute value of approximately 2.0 K (2.04 K). The above results preliminarily illustrate that the nadir direction is not the best observation angle by remote sensing for the direct acquisition of  $T_c$  in the case of only a single observation direction.

section 2.6.2 of  $T'(60, 180)$ ,  $T'(60, 300)$  and  $T'(60, 330)$ , the difference  $|\Delta T|$  is 1.43、1.11 and 1.51 K, respectively). Much smaller than the difference between  $T_0$  and  $T_c$  (the mean value of the difference is 2.89 K at these three moments). This is possible because when the view azimuth in the solar principal plane vertical orientation, the sensor can be more evenly to get the sunlight and shadowed face of the urban surface at the same time, so that the observed  $T(\theta, \varphi)$  can reflect more comprehensive information of  $T_c$ .

The above results have preliminarily indicated that the optimal observation azimuth is directly related to the position of the vertical plane of the solar main plane. Considering the influence of the ratio of building height to street width (H/W) on the thermal anisotropy (Krayenhoff et al., 2016), the H/W difference may also affect the location of the optimal observation position. So, we analyze polarization diagrams at all times, compare the difference of average absolute difference  $|\Delta T|_{\text{mean}}$  between four TUS, it is found that the azimuth of the best observation angular domain is still on the vertical plane of the solar main plane, and there are some differences in the zenith angle range. The H/W value of TUS02 and TUS04 is less than 1.0, the zenith angle of best viewing is approximately 45~60°, while the H/W value of TUS01 and TUS03 is greater than 1.0, the zenith angle of best viewing is approximately 30~60°, the differences are not difficult to understand, when H/W is large, the shadowed area of building increase, view zenith angle could be smaller to get more information of the wall temperature. In order to obtain the

optimal observation of general urban surface condition, further polarization diagram of average absolute difference  $|\Delta T|_{\text{mean}}$  between  $T_c$  and  $T(\theta, \varphi)$  of all scenarios is obtained (Fig.4).

This polarization diagram (Fig.4) shows that if the value of a domain (view) is smaller, the field tends to be closer to the  $T_c$ . In the hemisphere space, the range of  $|\Delta T|_{\text{mean}}$  is about 1.0~9.0 K. The value of  $|\Delta T|_{\text{mean}}$  is larger where the solar principal plane direction (the azimuth including toward and inverse to the sun) with larger zenith view angle (up to 5.5 K or more, that is not suitable as a view of approaching  $T_c$ ). In contrast, the value of  $|\Delta T|_{\text{mean}}$  is relatively small (it is only 1.2 K or less) where the view in the solar principal plane vertical azimuth and zenith angle is approximately 45~60°, this view can become optimal view of approaching  $T_c$ , as the results shown in Fig.3. Voogt and Oke (1997) did ground and flight observation in typical urban surface (including light industrial area, downtown and

residential areas), the observation of the position of the sun are mostly in the East direction (08:00~10:00, that in the early morning) or the West direction (15:00~17:00, that in the late afternoon), and fixed viewing zenith angle at 45°, the research shows that the azimuth angle is close to the North (near vertical surface at this time when the azimuth is located in the main plane of the sun),  $T(\theta, \varphi)$  can better approximate  $T_c$ . Although the structure and material of urban surface are different, the conclusion is similar to that of this study. The difference is that, due to the limitation of the cost of observation and conditions, Voogt and Oke (1997) demonstrated only the fixed viewing zenith angle is 45°, the viewing azimuth angle is located at the North direction is the best of the East, West, South and North direction. Through the complete simulation of the hemisphere space in the whole urban surface heat radiation, this paper gives the optimal observation under various scenarios of average.

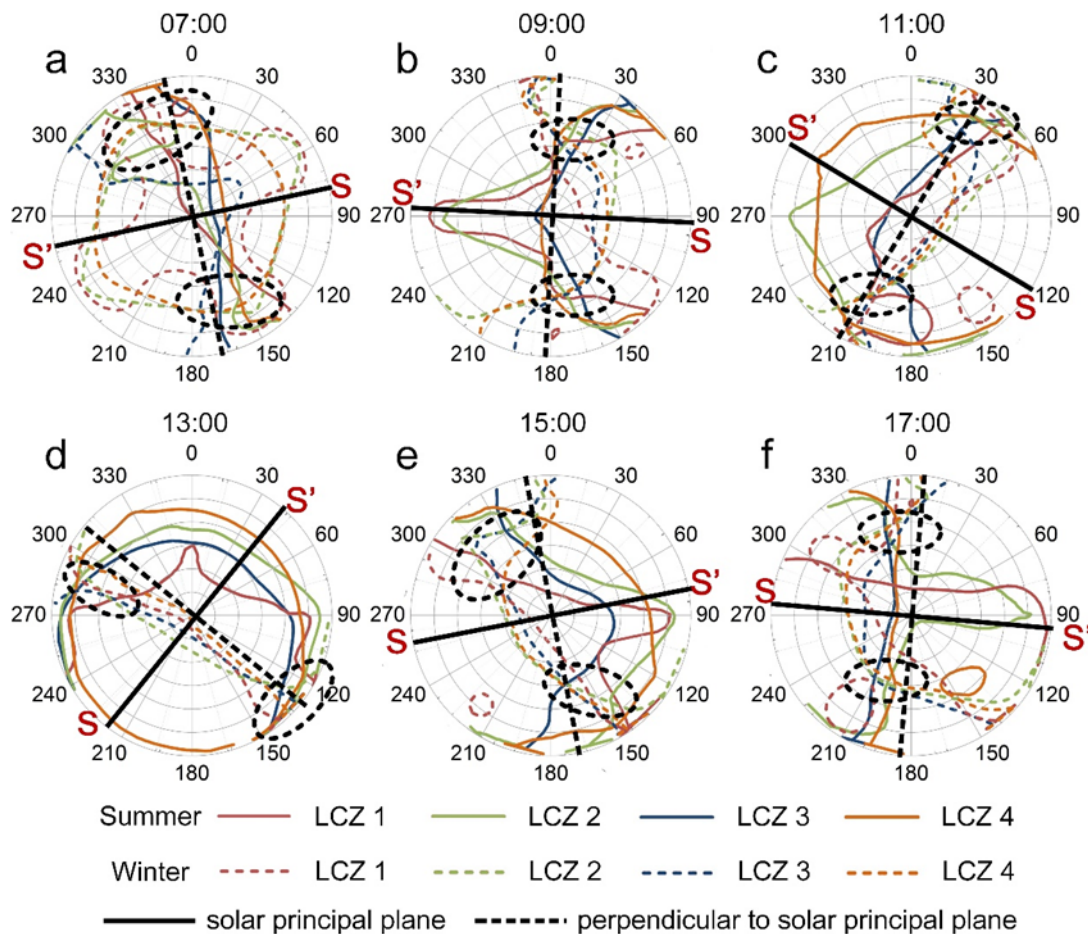
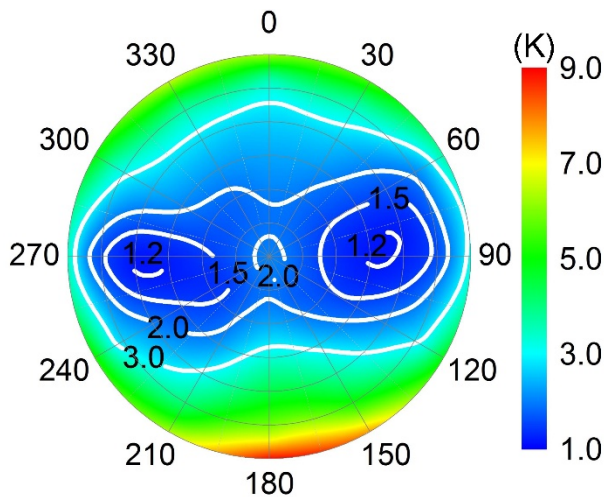


Fig.3 Contour line distribution of  $T_c$  in daytime. The range of the zenith and azimuth angle is consistent with Fig.2, and the black ellipse dotted circle is the area where the contour line is densely joined.



**Fig.4** The polar- $|\Delta T|_{\text{mean}}$  of average absolute difference between  $T_c$  and  $T(\theta, \varphi)$  (the sun azimuth is unified and rotated to the south).

### 3.3 Comparison of $T_H(\Omega)$ and $T_c$

The above is mainly given that the optimal observation field under the single observation direction  $T(\theta, \varphi)$ . In order to estimate  $T_c$  more accurately by remote sensing, this section focuses on how to use the integral temperature to get closer to the  $T_c$  with several  $T(\theta, \varphi)$ . This section selects the integral temperature mainly include  $T_{\text{oa}}$  (integral interval is the optimal view) and  $T_{\text{hx}}$  (integral interval is  $\theta \in [0, x], \varphi \in [0, 360]$ ). The comparison of  $T_H(\Omega)$  and  $T_c$  is shown in **Fig.5**.

Based on the daily variation of the difference between  $T_H(\Omega)$  and  $T_c$ , the following conclusions are obtained: (1) On the integral temperature, due to the strong effect of solar radiation during the daytime, the difference between sunlit and shadow component temperature is large, so  $|T_{\text{hx}} - T_c|$  is larger in the daytime, smaller at night, and the absolute difference is directly related to the value of the component temperature (or solar radiation). (2) The greater the range of the zenith angle integration  $[0, x]$ , the closer the  $T_{\text{hx}}$  is to  $T_c$ . In summer (**Fig.5.a**), for example, the average absolute difference  $|\Delta T|_{\text{mean}}$  between  $T_{\text{hx}}$  and  $T_c$ , with integral zenith angle increased from  $0^\circ, 30^\circ, 60^\circ$  and then increased to  $90^\circ$ , the value of  $|\Delta T|_{\text{mean}}$  from 1.33, 1.12, 0.84 K

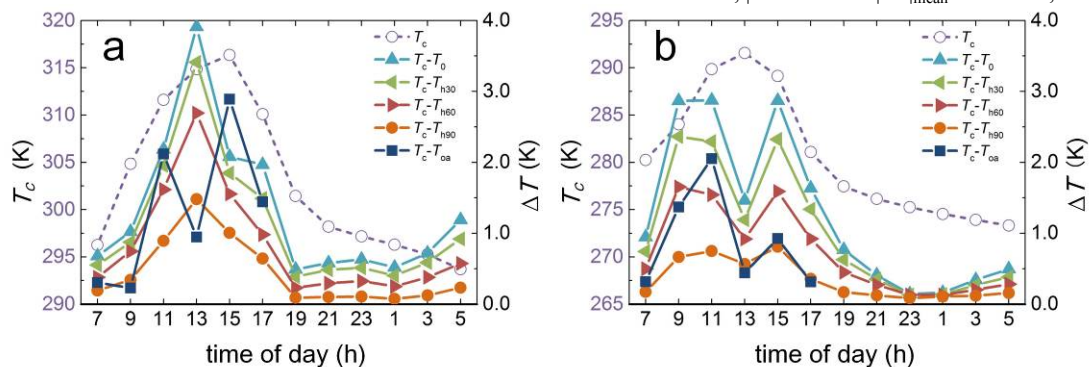


**Fig.5** Comparison of  $T_H(\Omega)$  and  $T_c$ . And, (a) and (b) indicate summer and winter, respectively.  $T_c$  is complete surface temperature,  $T_{\text{hx}}$  is integral temperature of the azimuth angle is from  $0$  to  $360^\circ$  and the zenith angle is from  $0$  to  $x$ ,  $T_{\text{oa}}$  is integral temperature of optimal view area. The vertical axis on the left and right shows the temperature value of  $T_c$  and the absolute difference between  $T_{\text{hx}}$ ,  $T_{\text{oa}}$  and  $T_c$ , respectively.

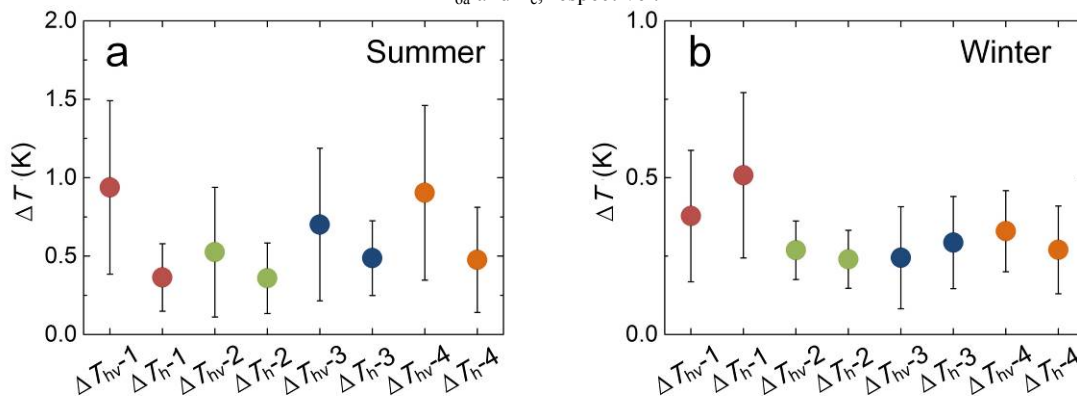


**Fig.6** Comparison of  $T_h$  based on kernel model and  $T_c$ . The Y-axis is the mean absolute difference  $|\Delta T|$  between hemisphere integral temperature and  $T_c$ , the circle represents the mean of  $|\Delta T|$  and the bound of 0.5 times standard deviation. The  $\Delta T_h$  is absolute difference  $|\Delta T|$  calculated from  $T_h$  (calculated by the original  $T(\theta, \varphi)$ ) and  $T_c$ , The  $\Delta T_{\text{hv}}$  is absolute difference  $|\Delta T|$  calculated from  $T_{\text{hv}}$  (calculated by  $T(\theta, \varphi)$  simulated by Vinnikov model) and  $T_c$ , the latter 1, 2, 3 and 4 represent 4 classes of TUS, respectively.

and then decreases to 0.44 K. In other words, hemisphere integral temperature  $T_{\text{h90}}$  can be the most accurate approximation of  $T_c$ , even in the summer, the lowest precision of 13:00, the difference between  $T_{\text{h90}}$  and  $T_c$  is only 1.48 K, and this accuracy is quite to most satellite surface temperature product. (3) The integral temperature  $T_{\text{oa}}$  which in a relatively narrow optimal view is slightly worse than  $T_{\text{h90}}$  in approaching  $T_c$ , but slightly

better than  $T_{\text{h60}}$ . In the daytime, the average absolute difference between the three integral temperature ( $T_{\text{oa}}$ ,  $T_{\text{h90}}$  and  $T_{\text{h60}}$ ) and  $T_c$  is 1.11, 0.66 and 1.26 K, respectively (**Fig.5**).

Hemisphere integral temperature covers the city surface radiation in all directions of thermal information, it can comprehensively reflect the real situation of all kinds of component temperature, which may be the important reasons can

be accurately approximated  $T_c$  (Roberts & Voogt, 2009). It is also shown that the integral temperature of a single narrow field of view (even the optimal observation horizon) is difficult to approximate the hemisphere integral temperature in terms of the ability to approach  $T_c$ .

#### 3.4 Comparison of $T_h$ based on kernel model and $T_c$

The above section shows that the hemisphere integral temperature  $T_{h90}$  (the following  $T_h$  for  $T_{h90}$  in this section) can be well approximated by  $T_c$ . However, the above  $T_h$  is mainly calculated from  $T(\theta, \varphi)$  in the forward simulation of the radiation directionality model. In general, forward modeling requires detailed surface geometry and component temperature information (Voogt, 2008; Lagouarde et al., 2011; Zhan et al., 2012). It is conceivable that such detailed structure and temperature information are difficult to obtain in remote sensing of urban thermal environment. Only by considering the thermal infrared remote sensing observation in a few directions, the  $T_h$  inversion can be carried out, and the estimation of  $T_c$  by remote sensing is feasible. In this section, we test the estimation of hemispheric integration temperature based on the kernel model (hereinafter referred to as Vinnikov model) developed by Vinnikov et al. (2012), and then estimate the approximation capability of the simulated hemisphere integration temperature to  $T_c$ . For this purpose, the  $T(\theta, \varphi)$  obtained from the section 2.6.2 is used to estimate the hemispheric integral temperature ( $T_{hv}$ ). Fig.6 shows the different types of TUS scenario, compares the difference value among  $T_c$  and  $T_h$  calculated from original  $T(\theta, \varphi)$  and  $T_{hv}$  calculated from Vinnikov model, that is  $\Delta T_h$  and  $\Delta T_{hv}$ .

From the dimensions of the physical scale model, the difference between  $\Delta T_h$  and  $\Delta T_{hv}$  is 0.39 ~ 0.97 K in summer, in contrast, the difference is smaller in winter, that is only 0.24~0.53 K. From the perspective of different moments of the day, the average values of  $\Delta T_h$  and  $\Delta T_{hv}$  are 0.76 and 1.44 K in the summer daytime (07:00~17:00), 0.12 and 0.19 K in the summer night (19:00~05:00). In winter, the average values of  $\Delta T_h$  and  $\Delta T_{hv}$  are 0.50 and 0.63 K in daytime (09:00~17:00), 0.13 and 0.17 K at night (19:00~07:00). Accordingly, the following conclusions are drawn: (1) Overall,  $T_h$  is closer to  $T_c$  than  $T_{hv}$ . (2) The difference between  $\Delta T_h$  and  $\Delta T_{hv}$  in all night time of summer and winter and winter daytime is so small that can be ignored, the difference is about 0.70 K in the summer daytime. Although  $T_{hv}$  is slightly worse than  $T_h$  in the  $T_c$  approximation ability, based on several (3~5)  $T(\theta, \varphi)$ ,  $T_{hv}$  is simply calculated by Vinnikov model while  $T_h$  need  $T(\theta, \varphi)$  of all directions in the hemisphere space, and average absolute difference of  $\Delta T_h$  and  $\Delta T_{hv}$  is only 0.13 K.

## 4 DISCUSSIONS

### 4.1 About precision

(1) Compared to  $|T_0 - T_c|_{\text{mean}}$  is about 2.0 K in the daytime,  $|T_{oa} - T_c|_{\text{mean}}$  is about 1.1 K,  $|T_{hv} - T_c|_{\text{mean}}$  is about 1.0 K, two methods provided in this paper are more accurate estimation of surface temperature. The process of land surface temperature inversion, influenced by the factors of emissivity, atmospheric effect, errors are inevitably introduced into the observation or simulation, several directional radiation temperature observations may introduce errors repeatedly, together with errors introduced during the simulation by kernel model, whether that estimation of  $T_c$  adopts a optimal angle observation is better. In fact, in satellite remote sensing observation, there are differences in solar positions at different times, it is difficult to

obtain  $T_{oa}$  at any time. So, in practical remote sensing observation,  $T_{oa}$  is used to represent  $T_c$  in the case of  $T_{oa}$  can be obtained, or there are several (3~5)  $T(\theta, \varphi)$ ,  $T_c$  is represented by the hemispherical integral temperature calculated by kernel model.

(2) At present, temperature inversion accuracy is low (about 2~3 K) by thermal infrared remote sensing in urban area, the approximation accuracy of  $T_c$  can reach 1.0 K in this paper, the relative accuracy on the angle dimension (accuracy of  $T(\theta, \varphi)$  and  $T_h$  approximation to  $T_c$ ), there is essential difference to the surface temperature inversion accuracy. In the follow-up study, even if the temperature inversion accuracy of urban area is increasing continuously, the temperature characteristics of urban underlying surface can not be accurately described if the directional difference caused by viewing angle can not be solved. Two methods for estimating  $T_c$  provided in this paper are mainly to solve the problem of angle dimension, and are able to bring the observation direction error to a minimum, to get the most close to the real urban surface temperature in the present remote sensing surface temperature inversion accuracy.

(3) Due to the complex three-dimensional structure of urban surface, the more change of sunlit or shadowed component surface, and rapidly changing temperature, it is difficult to obtain the detailed surface temperature in field measurement, and the error of time scale is difficult to eliminate. The models used in this paper (including land surface temperature simulation - Envi-met, directional radiation temperature simulation - CoMSTIR, kernel model simulation - Vinnikov model) are all classic models, simulation accuracy has been widely recognized. In addition, compared with the field observation conducted over a few days, land surface temperature of only a few areas can be obtained. This paper provides more data to analyze, find out the law and solve the scientific problems.

### 4.2 Shortages and prospects

The method proposed in this paper is simple and effective, can be used to estimate  $T_c$  accurately without detailed surface texture and component temperature information, and lays the foundation for the inversion of  $T_c$  by satellite remote sensing. Although some advances have been made in this paper, there are still some factors that may need further consideration: (1) It is not considered that emissivity of different surface types may vary greatly (for example, there is a significant difference between the emissivity of a metal component in a city building and a normal surface), and further research should be done to test the effect of component emissivity on estimation of  $T_c$ . (2) Based on the city "local climate division" system proposed by Stewart & Oke (2012), four typical urban surface types are tested in this paper, but it is difficult to fully characterize the urban surface types of cities all over the world. In particular, this paper does not consider adding vegetation components to the typical urban surface. Recent studies have shown that as the density of urban buildings changes, vegetation may increase or decrease the density of thermal anisotropy of urban surface (Dyce & Voogt, 2017). Nevertheless, the mechanism of the thermal anisotropy caused by urban buildings and vegetation is interlinked, it is conceivable that the basic conclusion of this paper should not change much after adding vegetation. (3) This paper only tested the classical Vinnikov kernel model for the reconstruction of directional radiation temperature. In fact, a number of kernel models which are more suitable for urban surfaces have been developed recently (Duffour et al., 2016). The application of these kernel models is expected to further improve the accuracy of estimating  $T_c$ . (4) This paper also confirmed that  $T_c$  is more representative of urban surface temperature. According to the estimation method of  $T_c$  provided here,  $T_c$  can be used to improve the estimation accuracy of heat island intensity (Allen et al.

2017), sensible heat flux and air temperature in urban area in the follow-up research work.

## 5 CONCLUSIONS

Traditionally, accurate estimation of complete urban surface temperature requires detailed surface 3D structural information with component temperature data. In this paper, the optimal observation angle (sight) of  $T_c$  (directional radiation temperature  $T(\theta, \varphi)$ ) is studied under the condition of only one observation, as well as in scenario, with multiple observations using the thermal radiation directionality kernel model to simulate the possibility of  $T_h$  close to  $T_c$ . The results show that: (1) in the case of only a single observation angle, in order to approach  $T_c$ , the optimal observation zenith angle of the sensor should be at 45–60°, and the observation azimuth should be near the vertical plane of the solar main plane. The quantitative calculation shows that the average absolute error of  $T(\theta, \varphi)$  and  $T_c$  is only 1.11 K when the observation angle (sight) is in the optimal observation angle. (2) As a complete characterization of the thermal radiation characteristics of urban surfaces in all directions, the hemispheric integral temperature  $T_h$  can be used instead of  $T_c$ , and its ability to approach  $T_c$  is superior to that of  $T(\theta, \varphi)$  at the optimum observation angle. (3) In the case of multiple directional thermal infrared observations, the hemispheric integral temperature based on the kernel model can also be used to directly substitute for  $T_c$ . About remote estimation of complete urban surface temperature, this paper provides a simple, accurate strategy, which is expected to serve the city surface atmosphere energy balance estimation, so as to promote and support the level of quantitative remote sensing of city thermal environment improvement. In addition, this paper is expected to provide a reference for further satellite orbit design for urban thermal environment observation.

## ACKNOWLEDGMENTS

This work is supported by the National Natural Science Foundation of China under Grants 41671420 and 41301360, and by the Key Research and Development Programs for Global Change and Adaptation under 2016YFA0600201. We are also grateful for the financial support provided by the DengFeng Program-B of Nanjing University.

## REFERENCES

- Adderley, C., Christen, A., & Voogt, J. A., 2015. The effect of radiometer placement and view on inferred directional and hemispheric radiometric temperatures of an urban canopy. *Atmospheric Measurement Techniques*, 8(7), 2699-2714.
- Allen, M. A., Voogt, J. A., & Christen, A., 2017. Towards a continuous climatological assessment of urban surface heat islands. In *Urban Remote Sensing Event (JURSE), 2017 Joint* (pp. 1-4). IEEE.
- Chow, W. T., Pope, R. L., Martin, C. A., & Brazel, A. J., 2011. Observing and modeling the nocturnal park cool island of an arid city: horizontal and vertical impacts. *Theoretical and Applied Climatology*, 103(1-2), 197-211.
- Duffour, C., Lagouarde, J. P., & Roujean, J. L., 2016. A two parameter model to simulate thermal infrared directional effects for remote sensing applications. *Remote Sensing of Environment*, 186, 250-261.
- Dyce, D. R., & Voogt, J. A., 2017. The influence of tree crowns on urban thermal effective anisotropy. *Urban Climate*.
- Fontanilles, G., Briottet, X., Fabre, S., Lefebvre, S., & Vandenhoute, P. F., 2010. Aggregation process of optical properties and temperature over heterogeneous surfaces in infrared domain. *Applied Optics*, 49(24), 4655-4669.
- Fontanilles, G., Briottet, X., Fabre, S., Trémas, T., & Henry, P. (2008, October). TITAN: a new infrared radiative transfer model for the study of heterogeneous 3D surface. In *SPIE Remote Sensing* (pp. 71070F-71070F). International Society for Optics and Photonics.
- Hénon, A., Mestayer, P. G., Groleau, D., & Voogt, J., 2011. High resolution thermo-radiative modeling of an urban fragment in Marseilles city center during the UBL-ESCOMPTE campaign. *Building and Environment*, 46(9), 1747-1764.
- Hu, L., Monaghan, A., Voogt, J. A., & Barlage, M., 2016. A first satellite-based observational assessment of urban thermal anisotropy. *Remote Sensing of Environment*, 181, 111-121.
- Huang, H., Xie, W., & Sun, H., 2015. Simulating 3D urban surface temperature distribution using ENVI-MET model: Case study on a forest park. In *Geoscience and Remote Sensing Symposium (IGARSS), 2015 IEEE International* (pp. 1642-1645). IEEE.
- Krayenhoff, E., & Voogt, J., 2016. Daytime thermal anisotropy of urban neighbourhoods: morphological causation. *Remote Sensing*, 8(2), 108.
- Lagouarde, J. P., & Irvine, M., 2008. Directional anisotropy in thermal infrared measurements over Toulouse city centre during the CAPITOU measurement campaigns: first results. *Meteorology and Atmospheric Physics*, 102(3), 173-185.
- Lagouarde, J. P., Hénon, A., Kurz, B., Moreau, P., Irvine, M., Voogt, J., & Mestayer, P., 2010. Modelling daytime thermal infrared directional anisotropy over Toulouse city centre. *Remote Sensing of Environment*, 114(1), 87-105.
- Lagouarde, J. P., Hénon, A., Irvine, M., Voogt, J., Pigeon, G., Moreau, P., Masson, V. & Mestayer, P., 2012. Experimental characterization and modelling of the nighttime directional anisotropy of thermal infrared measurements over an urban area: Case study of Toulouse (France). *Remote Sensing of Environment*, 117, 19-33.

- Li, Z. L., Tang, B. H., Wu, H., Ren, H., Yan, G., Wan, Z., ... & Sobrino, J. A., 2013. Satellite-derived land surface temperature: Current status and perspectives. *Remote Sensing of Environment*, 131, 14-37.
- Poglio, T., Mathieu-Marni, S., Ranchin, T., Savaria, E., & Wald, L., 2006. OSIRIS: a physically based simulation tool to improve training in thermal infrared remote sensing over urban areas at high spatial resolution. *Remote Sensing of Environment*, 104(2), 238-246.
- Ren, H., Yan, G., Chen, L., & Li, Z., 2011. Angular effect of MODIS emissivity products and its application to the split-window algorithm. *ISPRS Journal of Photogrammetry and Remote Sensing*, 66(4), 498-507.
- Roberts, S. M., & Voogt, J. A., 2009. Outdoor scale model experiment to evaluate the complete urban surface temperature. *Eighth Symposium on the Urban Environment*.
- Stewart, I. D., & Oke, T. R., 2012. Local climate zones for urban temperature studies. *Bulletin of the American Meteorological Society*, 93(12), 1879-1900.
- Soux, A., Voogt, J. A., & Oke, T. R., 2004. A Model to Calculate what a Remote Sensor Sees' of an Urban Surface. *Boundary-layer meteorology*, 111(1), 109-132.
- Vinnikov, K. Y., Yu, Y., Goldberg, M. D., Tarpley, D., Romanov, P., Laszlo, I., & Chen, M., 2012. Angular anisotropy of satellite observations of land surface temperature. *Geophysical Research Letters*, 39(23).
- Voogt, J. A., 2000. Image representations of complete urban surface temperatures. *Geocarto International*, 15(3), 21-32.
- Voogt, J. A., 2008. Assessment of an urban sensor view model for thermal anisotropy. *Remote Sensing of Environment*, 112(2), 482-495.
- Voogt, J. A., & Grimmond, C. S. B., 2000. Modeling surface sensible heat flux using surface radiative temperatures in a simple urban area. *Journal of Applied Meteorology*, 39(10), 1679-1699.
- Voogt, J. A., & Oke, T. R., 1997. Complete urban surface temperatures. *Journal of Applied Meteorology*, 36(9), 1117-1132.
- Voogt, J. A., & Oke, T. R., 2003. Thermal remote sensing of urban climates. *Remote sensing of environment*, 86(3), 370-384.
- Zhan, W., Chen, Y., Voogt, J. A., Zhou, J., Wang, J., Ma, W., & Liu, W., 2012. Assessment of thermal anisotropy on remote estimation of urban thermal inertia. *Remote Sensing of Environment*, 123(123), 12-24.
- Zhao, L., Gu, X., Yu, T., Wan, W., & Li, J., 2012. Modeling directional thermal radiance anisotropy for urban canopy. In *Geoscience and Remote Sensing Symposium (IGARSS), 2012 IEEE International* (pp. 3102-3105). IEEE.
- Ma, W., Chen Y. H., Zhan, W. F., & Zhou, J., 2013. Thermal anisotropy model for simulated three dimensional urban targets. *Journal of Remote Sensing*, 17(1), 62-76.
- Sun, H., Chen Y. H., Zhan, W. F., Wang, M. J., & Ma, W., 2015. A kernel model for urban surface thermal emissivity anisotropy and its uncertainties. *Journal of Infrared and Millimeter Waves*, 34(1), 66-73.
- Yu, T., Tian, Q. Y., Gu, X. F., Wang, J., Liu Q., & Yan, G. J., 2006. Modelling directional brightness temperature over a simple typical structure of urban areas. *Journal of Remote Sensing*, 10(5), 661-669.